Cell Genomics

Article

Synthetic chromosome fusion: Effects on mitotic and meiotic genome structure and function

Graphical abstract

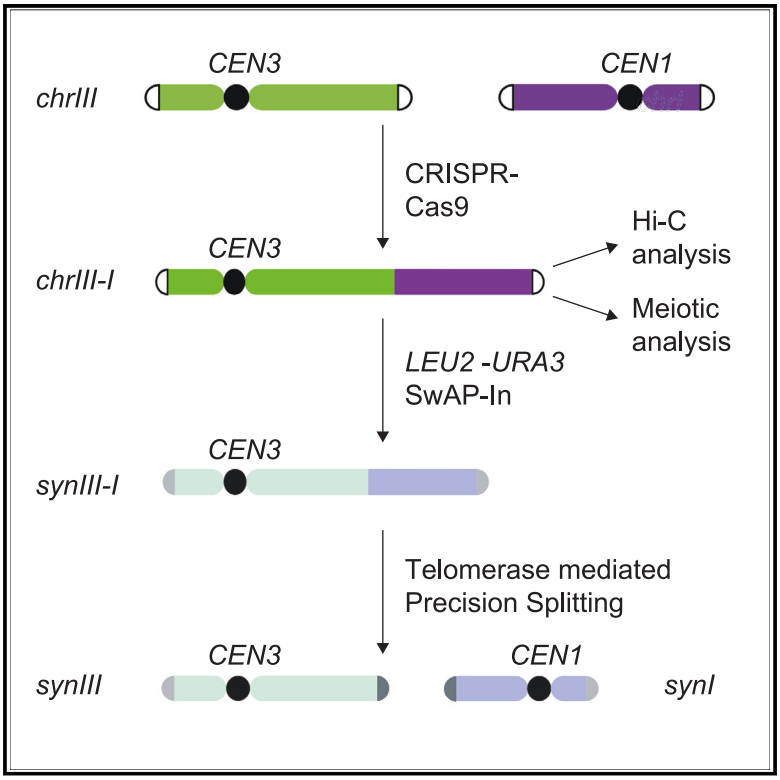

Highlights

- Developed different strategies to assemble/split synthetic fusion chromosomes
- Unexpected twisted structures in fusion chromosomes depend on Sir3 protein
- Centromere engineering revealed positive effects of centromeres on Red1 deposition

Authors

Jingchuan Luo, Luis A. Vale-Silva, Adhithi R. Raghavan, ..., Romain Koszul, Andreas Hochwagen, Jef D. Boeke

Correspondence

jef.boeke@nyulangone.org

In brief

Luo et al. develop new strategies to assemble synthetic fusion chromosomes and split fusion chromosomes. With this, they built yeast synthetic chromosome *I* ~21% shorter than the wild-type chromosome *I*, which grows well under a variety of growth conditions. They observed unexpected loops and twisted structures in some fusion chromosomes dependent on silencing protein Sir3. They also used fusion chromosomes to reveal a role of centromeres in positively recruiting axial elements and forming meiotic crossovers.

Luo et al., 2023, Cell Genomics *3*, 100439
November 8, 2023
https://doi.org/10.1016/j.xgen.2023.100439

CellPress

Cell Genomics

CellPress
OPEN ACCESS

Article

Synthetic chromosome fusion: Effects on mitotic and meiotic genome structure and function

Jingchuan Luo,[1,2] Luis A. Vale-Silva,[5] Adhithi R. Raghavan,[5] Guillaume Mercy,[3,11] Jonna Heldrich,[5] Xiaoji Sun,[1] Mingyu Kenneth Li,[1] Weimin Zhang,[1] Neta Agmon,[1] Kun Yang,[6,7] Jitong Cai,[7] Giovanni Stracquadanio,[6,7,8] Agnès Thierry,[3] Yu Zhao,[1] Camila Coelho,[1] Laura H. McCulloch,[1] Stephanie Lauer,[1] The Build-A-Genome Class, David B. Kaback,[10] Joel S. Bader,[6] Leslie A. Mitchell,[1] Julien Mozziconacci,[9] Romain Koszul,[3] Andreas Hochwagen,[5] and Jef D. Boeke[1,4,12,*]

[1]Institute for Systems Genetics and Department of Biochemistry and Molecular Pharmacology, NYU Langone Health, New York, NY 10016, USA
[2]Biochemistry, Cellular and Molecular Biology Graduate program, Johns Hopkins University School of Medicine, Baltimore, MD 21205, USA
[3]Institut Pasteur, CNRS UMR3525, Université de Paris, Unité Régulation Spatiale des Génomes, 75015 Paris, France
[4]Department of Biomedical Engineering, Tandon School of Engineering, Brooklyn, NY 11201, USA
[5]Department of Biology, New York University, New York, NY 10003, USA
[6]High Throughput Biology Center, Johns Hopkins University School of Medicine, Baltimore, MD 21205, USA
[7]Department of Biomedical Engineering and Institute of Genetic Medicine, Whiting School of Engineering, JHU, Baltimore, MD 21218, USA
[8]School of Biological Sciences, The University of Edinburgh, Edinburgh, UK
[9]Structure and instability of Genomes Lab, UMR 7196, Muséum National d'Histoire Naturelle (MNHN), 75005 Paris, France
[10]Department of Microbiology, Biochemistry and Molecular Genetics, Rutgers New Jersey Medical School, International Center for Public Health, Newark, NJ 07101-1709, USA
[11]Collège Doctoral, Sorbonne Université, 75005 Paris, France
[12]Lead contact
*Correspondence: jef.boeke@nyulangone.org
https://doi.org/10.1016/j.xgen.2023.100439

SUMMARY

We designed and synthesized *synI*, which is ~21.6% shorter than native *chrI*, the smallest chromosome in *Saccharomyces cerevisiae*. *SynI* was designed for attachment to another synthetic chromosome due to concerns surrounding potential instability and karyotype imbalance and is now attached to *synIII*, yielding the first synthetic yeast fusion chromosome. Additional fusion chromosomes were constructed to study nuclear function. *ChrIII-I* and *chrIX-III-I* fusion chromosomes have twisted structures, which depend on silencing protein Sir3. As a smaller chromosome, *chrI* also faces special challenges in assuring meiotic crossovers required for efficient homolog disjunction. Centromere deletions into fusion chromosomes revealed opposing effects of core centromeres and pericentromeres in modulating deposition of the crossover-promoting protein Red1. These effects extend over 100 kb and promote disproportionate Red1 enrichment, and thus crossover potential, on small chromosomes like *chrI*. These findings reveal the power of synthetic genomics to uncover new biology and deconvolute complex biological systems.

INTRODUCTION

Budding yeast has 16 linear chromosomes, with chromosome sizes ranging from 0.23 Mb to 1.5 Mb. The relatively small genome (12 Mb), a relatively high chromosome number (n = 16), and its unique life cycle (mitotic proliferation in both haploid and diploid states) make *Saccharomyces cerevisiae* a convenient model organism for a global synthetic eukaryotic genome project. The Synthetic Yeast Genome Project (termed Sc2.0) was launched in 2011 with the completion of the first synthetic chromosome arms, syn*IXR* and semi-syn*VIL*.[1] Since 2011, seven full-length synthetic yeast chromosomes have been successfully synthesized.[2–8] By building those synthetic yeast chromosomes, new insights into gene expression regulation and genome structure were revealed, as well as emphasizing the remarkable flexibility of the yeast genome that allow it to adapt to genetic changes.

Interestingly, even though there are thousands of designer changes in synthetic yeast chromosomes, the 3D structures of the synthetic chromosomes do not change much, except in the case of relocating ribosomal DNA (rDNA) arrays.[9] The relocation of rDNA from its native location—chr*XIIR* (a long arm) to chr*IIIR* (a short arm)—splits the chr*III* right arm into two non-interacting regions and imposes some new constraints on the nuclear genome. However, those synthetic yeast grow well even after rDNA relocation, indicating that yeast can tolerate big changes in nuclear 3D architecture. Whether such changes impact chromosomal behavior during specialized chromosomal configurations such as those observed in meiosis remains to be addressed. In other cases, yeast 3D structure was found to be related to its function. For example, distinct conformations of chromosome *III* observed in the two mating types may contribute to the donor preference phenomenon.[10] Thus, the role of yeast

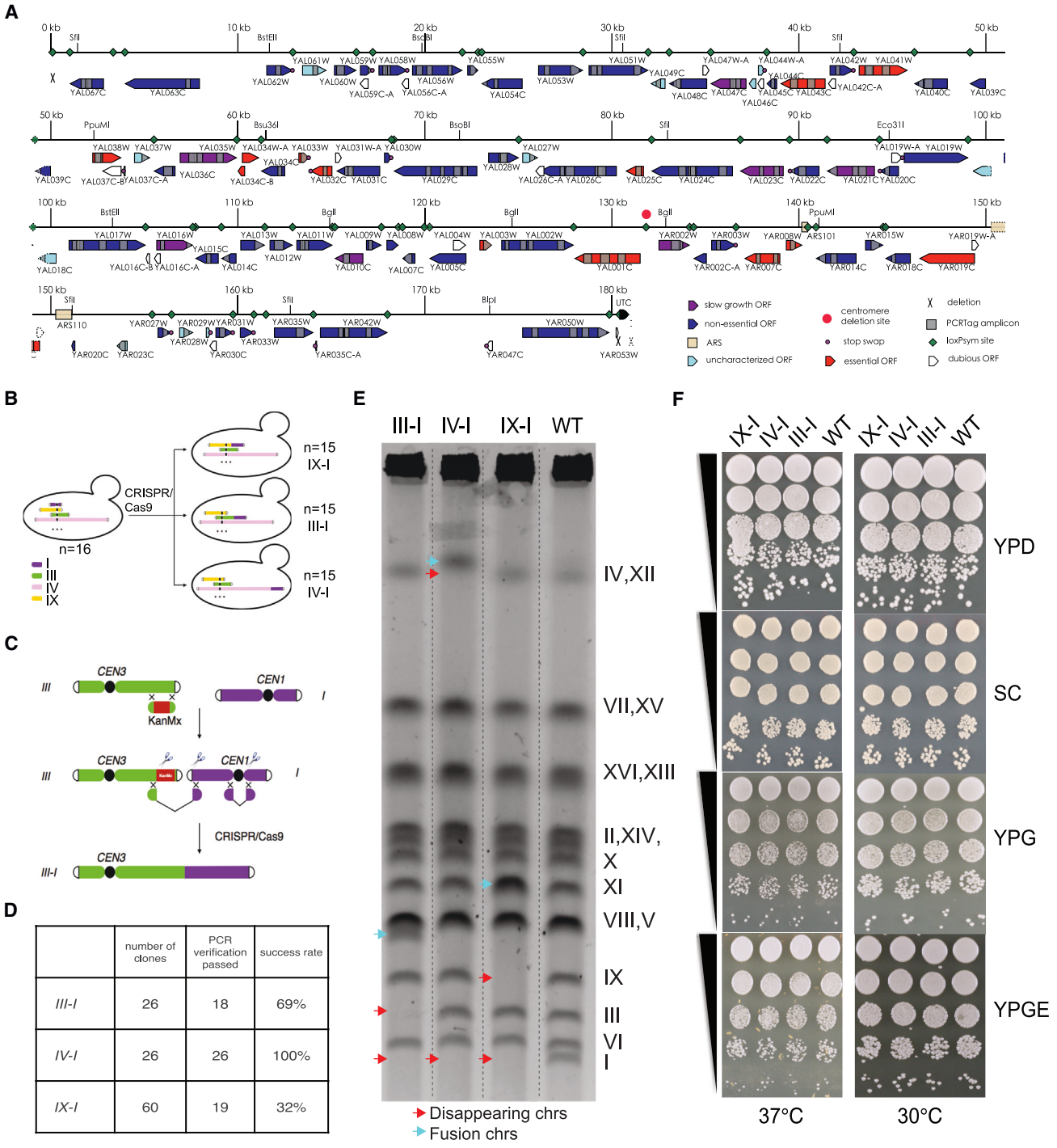

	number of clones	PCR verification passed	success rate
III-I	26	18	69%
IV-I	26	26	100%
IX-I	60	19	32%

Figure 1. The design of *synI* and construction and characterization of wild-type fusion chromosome strains

(A) *SynI* (180,554 base pairs) encodes all Sc2.0 design features, with a relative length reduction of 21.6% compared to wild-type *chrI*. Synthetic Universe Telomere Cap replaces the wild-type telomere, and the large deletions at subtelomeres are marked by "X." *CEN1* was removed, allowing *synI* to be attached to another synthetic chromosome. All retrotransposable elements and introns were deleted. tRNAs were relocated to neo-chromosome. Nineteen TAG stop codons were recoded to TAA, and 62 loxPsym sites were added to the 3′ UTR of non-essential genes and other major landmarks, such as telomeres and sites of tRNA and repeated DNA deletion sites.

(B) Schematic outlining the strategy used to construct *chrI* fusion strains.

(C) Schematic showing a CRISPR-Cas9 method deployed to fuse *chrI* to other chromosomes.

(D) The efficiency of the fusion chromosome method for *chrI*.

(legend continued on next page)

3D structure in transcriptome regulation and fitness remains of great interest.

During meiosis, small chromosomes in many sexually reproducing organisms, including humans, exhibit elevated rates of recombination.[11,12] In yeast, this chromosome size preference is reflected in the enrichment of several recombination-promoting proteins on small chromosomes (*chrs. I*, *III*, and *VI*).[13–15] Size preference is controlled by multiple pathways and is partly encoded in *cis*,[15–17] but the features that distinguish the small chromosomes are not well understood.

In this study, we complete the synthesis of synthetic chromosome *I* (*synI*), which is the smallest chromosome in wild-type yeast. Due to the concerns about potential chromosomal instability of *synI*, we attached *synI* to *synIII* and finished the assembly of the first fusion chromosome from scratch. We also generate a series of wild-type fusion chromosome strains to probe the impact of chromosome structure on three-dimensional genome structure as well as meiotic function. As the smallest chromosome, chromosome *I* faces special challenges in meiosis I in assuring meiotic crossovers required for its efficient disjunction in meiosis I. Here, we characterize the binding properties of axial element protein Red1 on the fusion chromosomes and provide evidence that far-ranging centromeric effects on Red1 deposition represent an important contributor to selective promotion of meiotic recombination in small chromosomes. Understanding these mechanisms is of importance for understanding what drives nondisjunction of small human chromosomes such as chromosome 21, which can lead to Down syndrome. In sum, through building and studying this synthetic chromosome, we were able to test the robustness of natural systems, deconvolute complex biological systems, and uncover new biological knowledge.

RESULTS

The design of *synI*

Compared to other Sc2.0 chromosomes, *synI* has many unique features. First, *synI* is dramatically shorter than its native counterpart (180,554 bp vs. 230,208 bp), yielding a relative length reduction of 21.6%. This contrasts with other synthetic chromosomes that are on average only 8% shorter than wild types.[18] This is due in large part to the removal of two ~10 kb subtelomere repeats, called W′ sequences, lacking coding sequences. It was previously suggested that W′ repeats might function as ''filler'' DNA, increasing the size and stability of this smallest yeast chromosome.[19] Since *chrI* is the smallest chromosome in *S. cerevisiae*, >6 times shorter than the largest chromosome (*IV*), we were concerned that further shortening it would negatively impact stability.[19,20] Thus, a second distinct design feature of *synI* is that it specifies attachment to another synthetic chromosome to help ensure its stability. To this end, *synI* lacks a centromere, and only the ''unattached'' right end is designed with a telomere. A second benefit of appending *synI* to another chromosome is that it balances the Sc2.0 karyotype at n = 16, which would otherwise be increased by 1 due to planned introduction of a supernumerary tRNA neochromosome.[18]

Besides these unique properties, *synI* design adhered to general principles laid out for Sc2.0 chromosomes[1,18] (Figure 1A). Specifically, four tRNA genes, all introns, and all retrotransposon sequences were deleted. Further, 3,535 bp were recoded as PCRTags, enabling distinction of synthetic and wild-type DNA in PCR-based assays,[1] and 210 bp were recoded to create or eliminate restriction enzyme cut sites used for chromosomal assembly. Nineteen TAG stop codons were swapped to TAA, and 62 loxPsym sites were added 3 bp downstream of non-essential gene stop codons, and also at other major landmarks, such as telomeres and sites of tRNA and associated repeat deletion.

Strategy to fuse *synI* to three different chromosomes

The first major decision to be made prior to *synI* construction was the chromosome to which it should be attached. We did not know whether the altered 3D environment forced by such an attachment would affect *chrI* performance, so we set out to fuse *chrI* to three chromosomes with distinct arm lengths: *chrIIIR*, *chrIVR*, and *chrIXR* (Figure 1B). *chrIXR* is the shortest arm in *S. cerevisiae* at ~84 kb, whereas *chrIVR* is the longest arm (excluding the variable-length rDNA locus on chromosome *XII*) at over 1 Mb. *ChrIIIR* has an intermediate length of ~202 kb. To evaluate the performance of these fusion chromosomes, we used native chromosomes.

Characterization of native fusion chromosomes

To fuse chromosomes in *S. cerevisiae*, we used a previously developed variation of a CRISPR-based method that allows, in principle, fusion of *chrI* to any other chromosome (Figure 1C).[21] For *synI*, this method was very robust; success rates varied from 32% to 100% (Figure 1D). Pulsed-field gel electrophoresis was used to determine molecular karyotypes (Figure 1E). *ChrI* and its fusion partners (*chrIII*, *chrIV*, or *chrIX*) showed the expected slower-migrating bands (*chrIII-I*, *chrIV-I*, or *chrIX-I*). To evaluate the growth fitness of the three fusion chromosome strains, serial dilution spot assays in different media and temperature conditions were performed (Figure 1F). Under all conditions tested, fusion chromosome strains grew as well as wild type, without notable differences.

Assembly of *synI*

The high fitness of the fusion chromosome strains indicates that attachment of *chrI* to different-length chromosome arms does not affect its overall performance. To move ahead with synthesis and assembly, we attached *chrI* to *synIII* for two reasons. First, *synIII* was successfully assembled, had high fitness, and was available at that time, whereas *synIX* and *synIV* were still under construction. Moreover, *synIII* demonstrates high fitness under

(E) Pulsed-field gel electrophoresis. Fusion chromosome strain names are indicated atop the gel image. WT, wild-type strain. Red arrows = former location of wild-type chromosomes; blue arrows = new fusion chromosomes.

(F) Serial dilution assays to evaluate fitness of fusion chromosome strains. YPD, yeast extract peptone dextrose; SC, synthetic complete medium; YPG, yeast extract peptone with 3% glycerol; YPGE, yeast extract peptone with 3% glycerol and 3% ethanol.

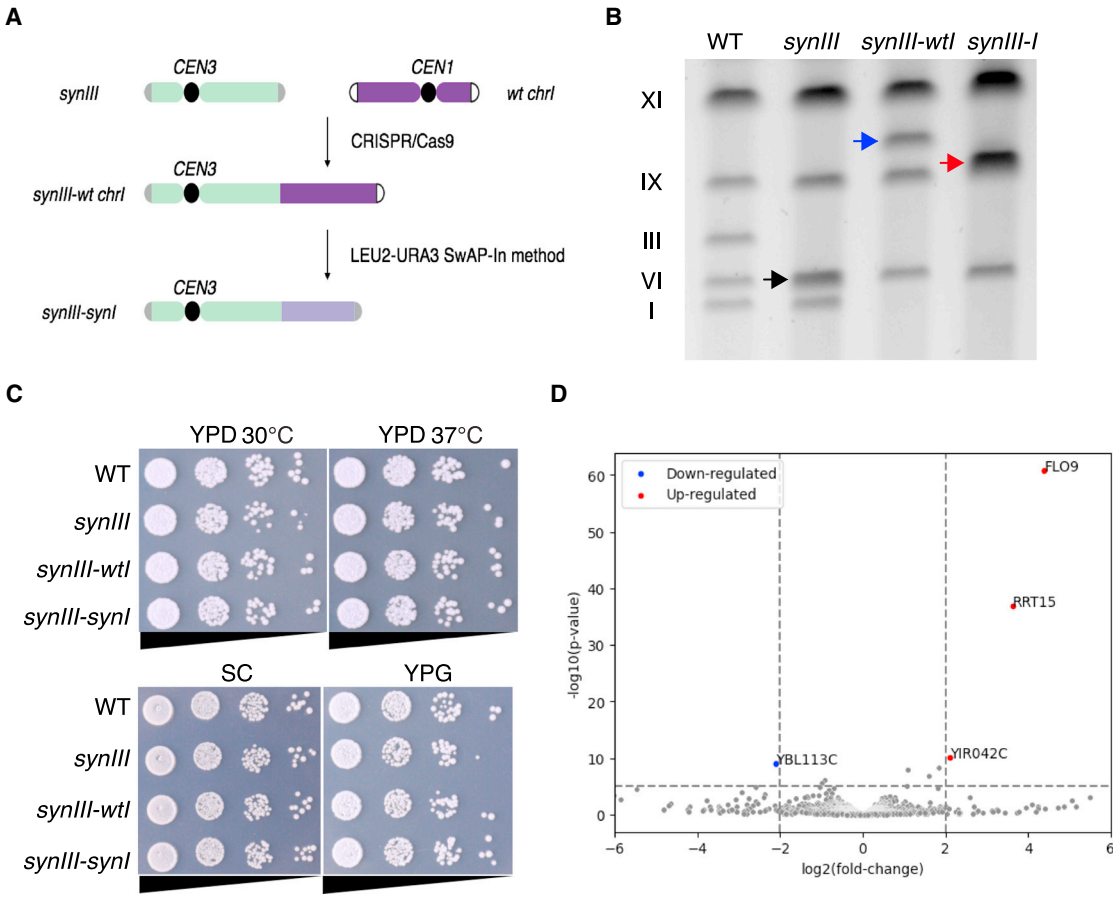

Figure 2. Construction and characterization of *synIII-I*

(A) Schematic showing the strategy to assemble synthetic chromosome *I*.

(B) Pulsed-field gel electrophoresis result. *SynIII* (~273 kb, indicated by a black arrow) migrates faster than wild-type *chrIII* (~317 kb) and co-migrates with wild-type *chrVI* (~270 kb). The attachment of wild-type chromosome *I* to *synIII* creates a slower-migrating chromosome (~496 kb), indicated by a blue arrow. The red arrow indicates the size of the *synIII-I* fusion chromosome (~453 kb), which migrates faster than *synIII-wtI*.

(C) Serial dilution growth assay. YPD, yeast extract peptone dextrose; SC, synthetic complete medium; YPG, yeast extract peptone with 3% glycerol.

(D) A volcano plot showing RNA-seq data comparing the transcriptome of *synIII-I* and *synIII-wtI* strains. Red and blue dots indicate genes whose expression is significantly different in the *synIII-I* strain compared to *synIII-wtI* strain. $p < 10^{-5}$, $|\log_2(\text{fold change})| > 2$.

more than 20 conditions, including elevated temperatures, DNA replication stress, DNA damage stress, and oxidative stress.[2] To assemble *synI*, we started with a *synIII-wtI* fusion chromosome strain, containing *CENIII* as the sole centromere. This enabled subsequent use of the "switching auxotrophies progressively for integration" (SwAP-In) method, allowing replacement of wild-type *chrI* with synthetic DNA in a series of five steps subsequent to fusion with *synIII* (Figure 2A).[18]

After attachment of native *chrI* to synthetic *chrIII*, and five consecutive megachunk integrations, the ~180 kb synthetic chromosome *I* was completed. PCRTags were used to detect the replacement of wild-type genome by synthetic sequences (Figures S1 and S2). Pulsed-field gel electrophoresis demonstrated that we successfully assembled fusion chromosome *synIII-I* (Figure 2B). *SynIII* migrates faster than wild-type *chrIII* due to an ~44 kb reduction in total length. In the *synIII-wtI* fusion strain, both *chrI* and *synIII* bands relocate to the predicted electrophoretic mobility of the synthetic fusion chromosome. The *synIII-I* chromosome (~453 kb) co-migrates with *chrIX* (~440 kb). During assembly, we identified a handful of synthetic features that caused apparent fitness defects, and we elected to keep the wild-type sequence to preserve high fitness (Table S1). Besides a growth defect on high sorbitol concentrations that may originate from the parent strain *synIII*,[2] the fusion chromosome strain *synIII-I* grew without any defect compared to wild-type control strains. This is notable despite the >20% reduction in *chrI* length and removal of W′ repeats (Figures 2C and S3). Subsequently, we utilized the telomerator,[22] initially developed in our lab, as part of a "precision chromosome splitting" strategy to reintroduce wild-type *CEN1* and divide the *synIII-I* chromosome into two independent synthetic chromosomes: *synIII* and *synI* (Figure 3A). We used both PCR and pulsed-field gels to verify the separation of *synI* from *synIII* (Figures 3B and 3C). The resulting strain with individual *synI* (a mere ~180 kb long) grew comparably to the wild type on rich medium (Figure 3D).

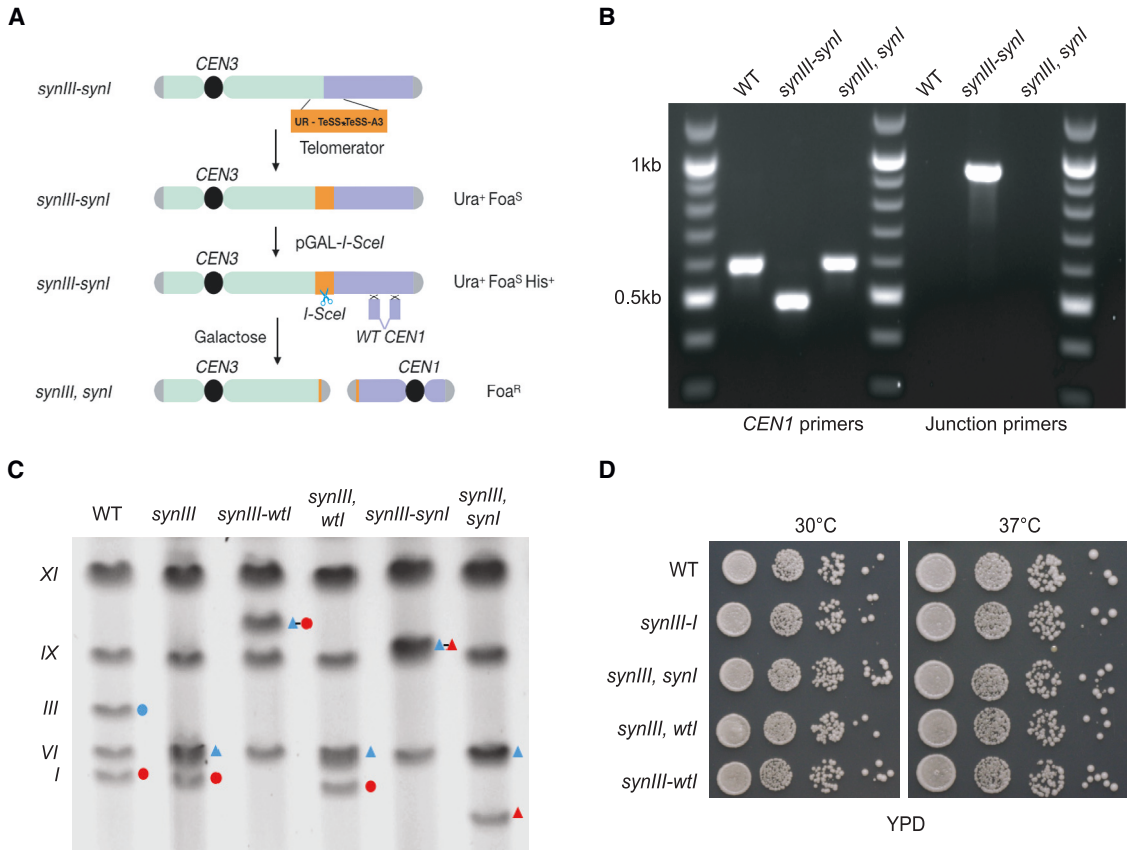

Figure 3. Construction and characterization of "liberated" *synI*

(A) Schematic illustrating the "telomerase mediated precision splitting" strategy to separate the synthetic chromosome *III-I* into two synthetic chromosomes *III* and *I*. The telomerator contains a *URA3* gene with an *ACT1* intron, which has an endonuclease *I-SceI* recognition site (indicated as *) flanked by telomere seed sequences (TeSS).

(B) PCR results with primers spanning the *synIII-I* junction and *CEN1*. The amplicon for junction PCR is 938 bp. The amplicon for wild-type *CEN1* is 603 bp, while it is 519 bp in the *synIII-I* strain with *cen1Δ*.

(C) Pulsed-field gel electrophoresis results. Synthetic chromosomes are marked by triangles, wild-type chromosomes by dots. Blue represents *chrIII*, and red denotes *chrI*. *SynIII* (~273 kb) comigrates with wild-type *chrVI* (~270 kb), while *synIII-synI* (~453 kb) comigrates with wild-type *chrIX* (~440 kb).

(D) Serial dilution growth assay. YPD, yeast extract peptone dextrose.

We performed whole-genome sequencing to detect potential genome variation and RNA sequence (RNA-seq) profiling to detect potential transcriptome changes. DNA sequencing of the *synIII-I* genome revealed a few SNPs and indels in *synI* compared to the designed genome (Table S2). RNA-seq revealed only four genes whose expression changed significantly. Among these, two are putative proteins with unknown function (*RRT15* and *YIR042C*), and one encodes a helicase-like protein within the telomeric Y′ element on chromosome 2 (*YBL113C*). Another, located on *synI* itself, encodes a lectin-like protein involved in flocculation (*YAL063C-FLO9*) (Figure 2D). The expression of *YBL113C* was significantly reduced, whereas *FLO9* increased expression substantially. *FLO9* is located on the left arm of *chrI*, near the *chrIL* telomere. In the *synI* design, *FLO9* was recoded (using "REPEATSMASHER"[18]) to facilitate proper assembly because native *FLO9* contains tandemly repeated peptide sequences.[22] Prior work has shown that telomere-located genes are overexpressed when the telomere is fused to another chromosome[21,23] or the chromosome is circularized.[3,6] However, it is possible that extensive recoding of *FLO9* contributes to its increased expression.

Chromosome fusion does not affect overall 3D genome structure

To investigate potential changes of 3D nuclear architecture in wild-type fusion chromosome strains, we exploited Hi-C to study three-dimensional organization.[24] Native yeast genome organization adopts a Rabl-like configuration: a polarized array with 16 centromeres held together by tethering to the spindle pole body, and telomeres clustering within the opposing hemisphere[25]; chromosome arms of similar length interact more extensively.[26] Fusing *chrI* to other chromosomes did not change overall Rabl configuration (Figure 4A). As expected, attachment of *chrI* to another chromosome significantly increased both local and global (i.e., non-adjacent) interactions between *chrI* and the attached chromosome,

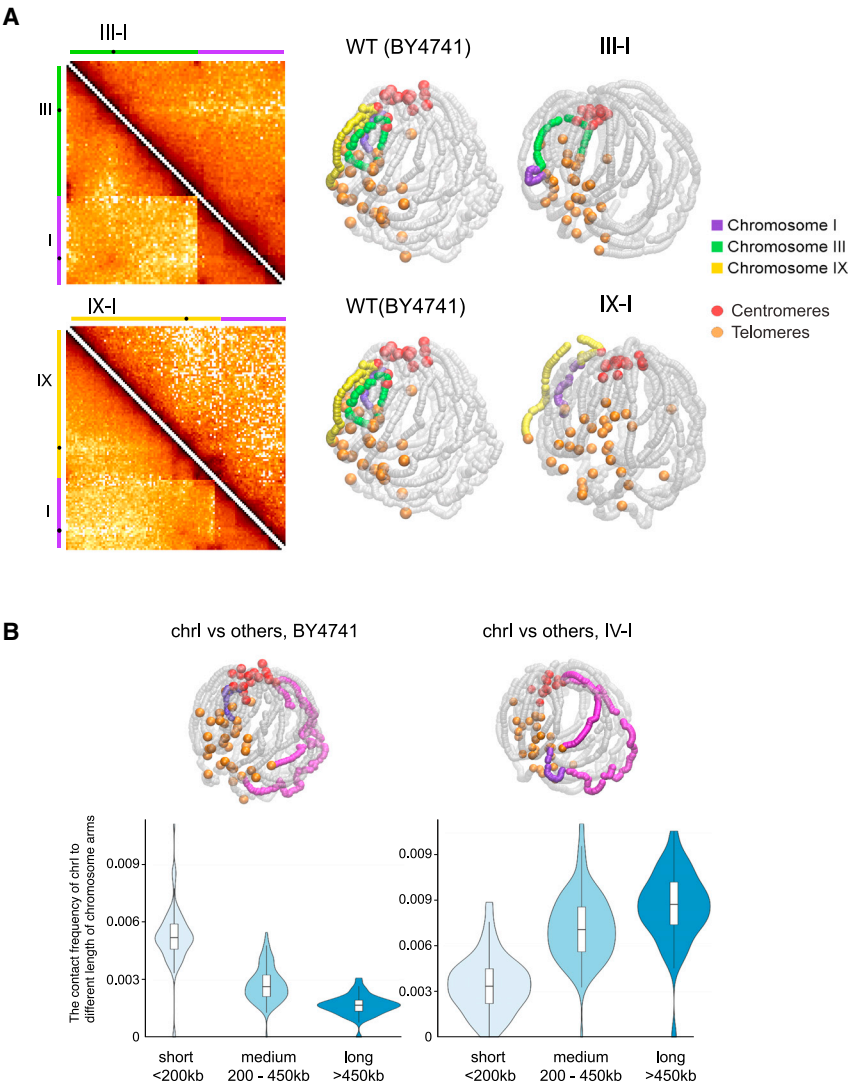

Figure 4. 3D genome organization of wild-type fusion chromosome strains

(A) Comparisons of normalized contact maps of fusion chromosome strains and wild-type strains (5 kb bin) and 3D representations inferred from Hi-C contact maps.

(B) Violin plots showing the contact frequency of *chrI* to short (<200 kb), medium (200–400 kb), or long (>400 kb) chromosomal arms, for the wild-type strain (BY4741) and for the strain with *chrI* fused to the long arm of *chrIV*. 3D representations are shown in the top of violin plots for visualization comparison; *chrI* is represented in purple and *chrIV* in pink; centromeres are colored in red and telomeres in orange.

indicated by higher contact frequency in 2D maps (Figure 4A). An increased frequency of inter-chromosome interactions with chromosome arms of similar lengths to the "fusion arm" was also noted. In the most dramatic case, namely the *chrI-chrIV* fusion, *chrI* interacted much more with long arms than short arms, revealing a completely different trend from the one in wild-type yeast (Figure 4B). We note that the contact maps and 3D representations are averages derived from a population of nuclei[27]; individual nuclei may well display dynamic and diverse genome architecture.

The *chrIX-III-I* fusion chromosome displays a Sir3-dependent complex twisted structure

In comparison to the native genome, in which *chrI* stretches out in typical Rabl configuration, in the *chrIII-I* fusion we observed an unexpected loop forming between the *chrIR* telomere and the fusion point, proximal to *HMR* on *chrIII* (Figure 5A, *chrIII-I* strain). We did not see this loop in the *chrIX-I* fusion chromosome strain, suggesting that *cis*-sequences on *chrIII* are required for its formation. *HML* and *HMR* are silent mating type cassettes, located near the left and right ends of *chrIII*, respectively, silenced by the SIR protein complex.[28] In *chrIX-III-I*, which was generated by fusing *chrIXR* to the left arm of *chrIII-I*, the chromosomal fusion points represent positions at which *HML* and *HMR* interact (Figure 5A). The 3D representation suggests that the *chrIXR* sequences cross between *chrIR* and *HMR* sequences and are extruded, forming a complex twisted structure. This interaction pattern could be explained by a strong *HML-HMR* interaction, leading to a geometric block of the *chrI* telomere loop. Interestingly, these novel twisted/looped structures were absent from the *sir3Δ* variant of the *chrIX-III-I* strain, consistent with dependence on the SIR complex in formation and/or maintenance of this 3D structure. The comparison map between *SIR3* and *sir3 chrIX-III-I* strains revealed that interactions between *chrIX* and *chrI* or *chrIII* were much stronger in *SIR3* strains (Figures 5B and 5C).

Preferential Red1 binding to small chromosomes is mediated by centromeres

The fusion chromosomes also provided an opportunity to investigate the unique meiotic behavior of small chromosomes. Formation of crossovers (chiasmata) is crucial to proper segregation in meiosis I. Small chromosomes have fewer opportunities to cross over/recombine with homologs due to their short length, and years of study have shown that there is a special but poorly characterized mechanism to promote enrichment of several recombination-promoting proteins on the three smallest chromosomes (chrs *I*, *III*, and *VI*) to make sure that they form chiasmata and separate properly during meiosis.[11,13–17] To investigate the mechanism, we analyzed a series of fusion chromosomes for patterns of binding of axial element protein Red1, among the most upstream recombination factors known to be differentially enriched on small chromosomes.[13,14] To

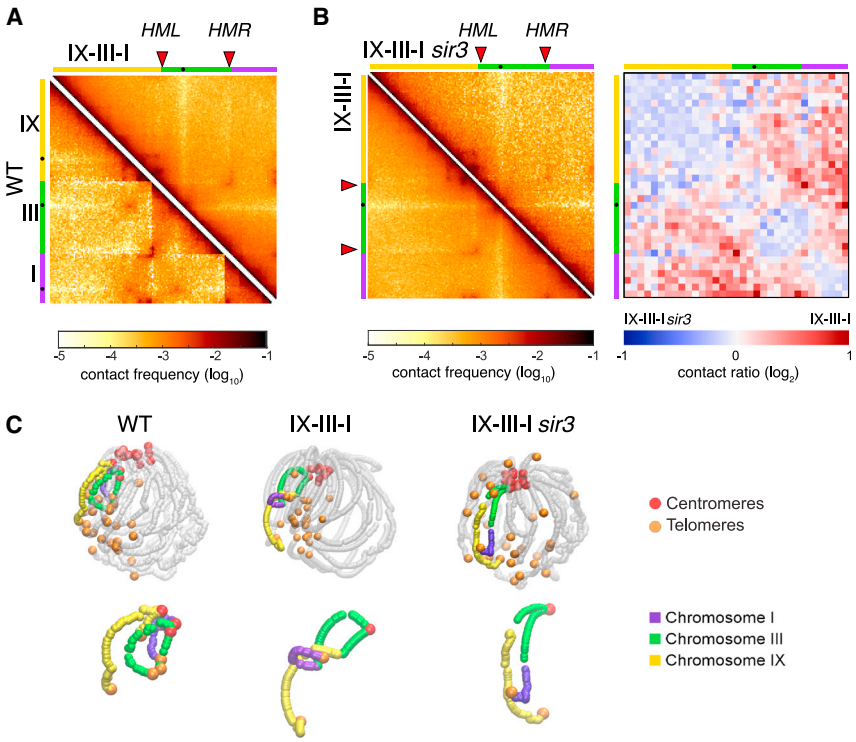

Figure 5. Twisted structure formed in *chrIX-III-I* is Sir3 dependent

(A) Comparisons of normalized contact maps of wild-type strains and *chrIX-III-I* strains. Red arrows point at *HML* and *HMR* loci.

(B) Comparisons of normalized contact maps of *chrIX-III-I* strains with or without Sir3 protein. Left panel: normalized contact maps. Right panel: ratio between two contact maps (50 kb bin). Blue contacts are stronger in the *chrIX-III-I sir3* strain; red contacts are stronger in the *chrIX-III-I* strain.

(C) 3D representations inferred from the contact maps using Shrek 3D.[27] The blank spaces in the junctions on *chrIX-III-I sir3* strain reflect the lower mappability of subtelomeric sequences, which were excluded from subsequent analysis.

bypass the poor sporulation efficiency of BY4741,[29] this experiment was performed in hybrid BY4741/SK1 strains. The presence of the same SK1 genome in all hybrids provided an internal control of ChIP-seq efficiency, allowing normalization between samples.

ChIP-seq analysis showed the expected over-enrichment of Red1 on the three smallest chromosomes (*chrI*, *chrIII*, and *chrVI*) for both BY4741 and SK1 alleles (Figures 6Ai and S4). Strikingly, the same biased enrichment was also observed within the context of fusion chromosomes. Red1 was enriched on *chrI* sequences within the much larger *chrIV-I* chromosome (in which *chrI* is attached to *chrIV* and *CEN4* is deleted; Figure 6Aii) and on *chrIII* sequences within the *chrIX-III-I* fusion chromosome (which has an intact *CEN3*; Figure 6Av), despite the massive size increase resulting from these fusions. These data demonstrate that Red1 enrichment on small chromosomes is, to a large extent, encoded in *cis*.

Deletion analysis revealed that Red1 enrichment on *chrI* sequences was linked to the presence of *CEN1*. When *CEN1* instead of *CEN4* was deleted from the *chrIV-I* fusion chromosome, the biased Red1 enrichment on *chrI* sequences was largely abolished (Figure 6Aiii). Substantially less biased enrichment on *chrI* sequences was also observed for *chrIX-III-I* fusion chromosomes lacking *CEN1* (Figure 6Aiv and v). Thus, sequences within the 118-bp core sequence of *CEN1* are needed to increase Red1 levels on *chrI*. A similar effect was also observed upon disruption of *CEN3*, although the effect was less pronounced, possibly because of redundant elements elsewhere on *chrIII* or because only three critical base pairs of *CEN3* were deleted, leaving much of the core *CEN3* sequence intact (Figure 6Aiv).

Long-range effects of centromeres on Red1 enrichment

Analysis of Red1 distribution along chromosomes revealed a highly reproducible local drop in Red1 signal intensity whenever *any* centromere was deleted in the context of a fusion chromosome (Figures 6B, 6C, and S4). For example, when *CEN9* was retained in the construction of *chrIX-III-I*, we observed a drop in overall Red1 signal around the inactivated *CEN3* and deleted *CEN1* but no drop around *CEN9*. Conversely, when *CEN3* was retained in the construction of *chrIX-III-I*, the signal dropped only around the deleted *CEN1* and *CEN9*. This effect is also seen for *CEN4* in the *chrIV-I* fusion chromosome (Figures 6C and S4) and thus also occurs at centromeres of large chromosomes.

Indeed, plotting signal within Red1 peaks as a fraction of wild type revealed a decrease in Red1 signal across a ~200 kb region centered on the deleted centromeres (Figure 6C). A similar drop in binding signal was also observed when the *chrIV-I* fusion was made homozygous for both BY4741 and SK1 genomes, thus excluding indirect effects from hemizygosity in the hybrid strains (Figure S5). The range of this effect is extraordinary given that in some cases just three nucleotides were mutated to inactivate a centromere (Table S4). These data suggest that the drop in Red1 signal is a consequence of losing centromere activity rather than alterations of base composition or other larger-scale consequences of sequence deletion. We conclude that centromere activity acts in *cis* to promote Red1 binding over distances large enough to nearly encompass the entirety of the smallest yeast chromosomes.

Somewhat unexpectedly, centromere inactivation actually led to a drop of Red1 levels below the genome average, implying that the pericentromeric regions have a lower overall intrinsic propensity to recruit Red1 than the rest of the genome. To separate the effects of centromeres and pericentromeres, we took advantage of the recently engineered "inside out" *synIV* chromosome[8] in which *CEN4* was relocated to a new position at the former site occupied by the two telomeres, exploiting circular intermediates (Figure 7A). As a result, the sequences near the new *CEN4* were originally adjacent to the telomeres. ChIP-seq

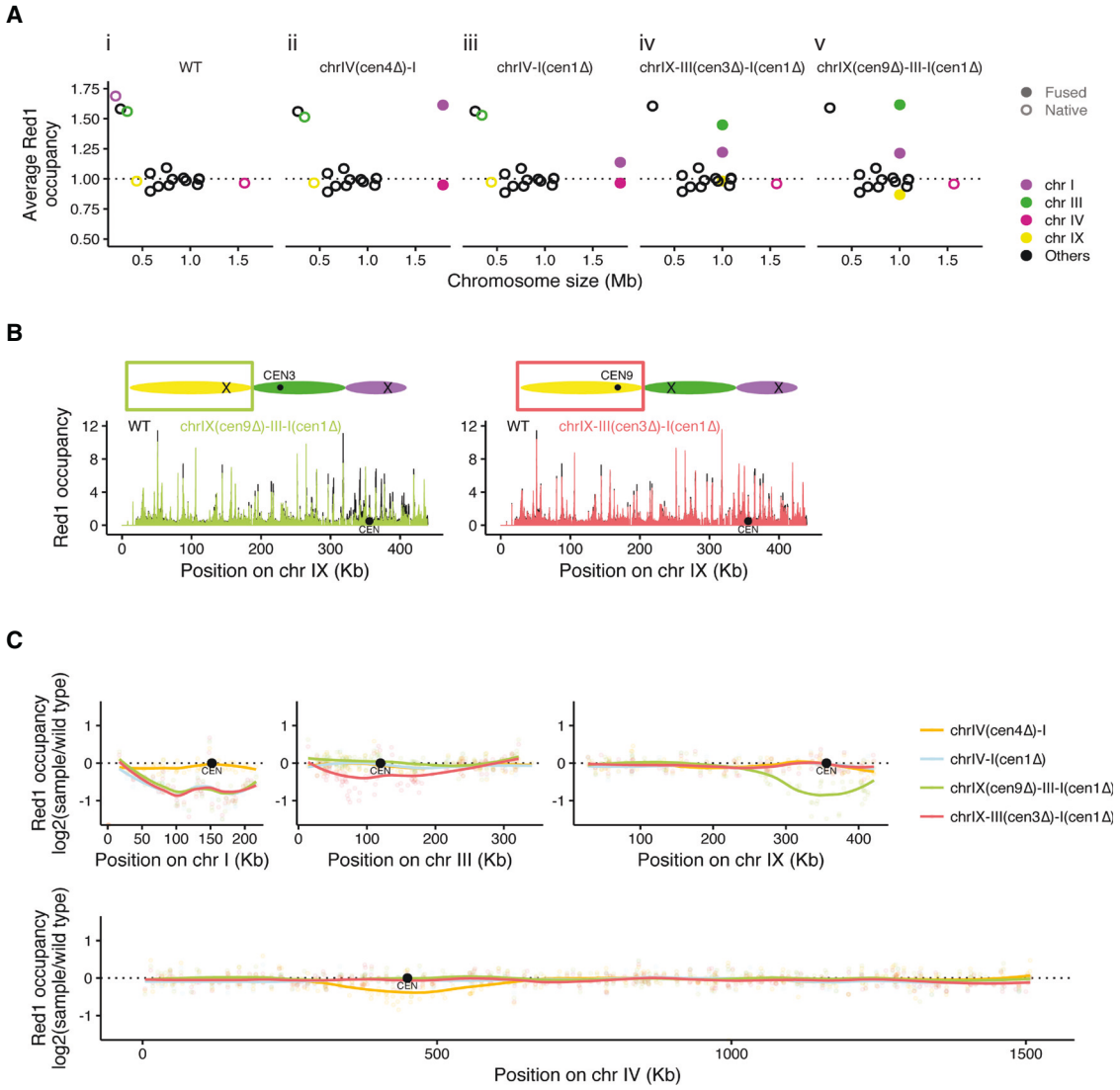

Figure 6. Distribution of the meiotic axis protein Red1 along fusion chromosomes in heterozygous SK1/S288c hybrid strains

(A) Red1 occupancy versus chromosome length in the S288c background. Panels: i, wild type; ii, fusion chromosome *IV-I* with *cen4Δ*; iii, fusion chromosome *IV-I* with *cen1Δ*; iv, fusion chromosome *IX-III-I* with *cen1Δ* and inactive *cen3*; v, fusion chromosome *IX-III-I* with *cen1Δ* and *cen9Δ*. Chromosomes in fusion chromosomes are indicated by filled circles while wild-type chromosomes are indicated by circles.

(B) Red1 occupancy along S288c *chr IX* for each fusion chromosome strain (colored) overlaid on the wild-type occupancy (black).

(C) Mean signal in Red1 peaks along fusion chromosomes as $\log_2$-transformed ratios between each strain and the wild type. Points represent mean peak signal and lines represent local regression (loess normalized).

analysis of these chromosomes showed the expected depletion of Red1 signals around the location of the original *CEN4* but also revealed a significant increase of Red1 signals surrounding the transplanted *CEN4* position, i.e., the new "ectopic" pericentromere (Figures 7A and S6), while leaving overall Red1 binding levels unchanged (Figure 7B). These data show that centromeres suffice to establish large regions of Red1 enrichment and imply that the pericentromeric sequences have actually adapted to reduce this recruitment.

To investigate whether patterning of Red1 was reflected in the recombination landscape, we analyzed homozygous *chrIV-I* fusion strains lacking either *CEN4* or *CEN1*. Analysis of genetic intervals to the right of *CEN4* revealed reduced rates of recombination in the first ~100 kb from *CEN4* compared to the more distal interval, consistent with inherent suppression of recombination in this region (Figure S7). This suppression was observed regardless of the presence of *CEN4*, indicating that the depression of Red1 signal seen in the absence of *CEN4* does not cause a further decrease in meiotic recombination in the pericentromeric region.

DISCUSSION

In this study, we finished assembling the first synthetic yeast fusion chromosome from scratch. Strains carrying this fusion

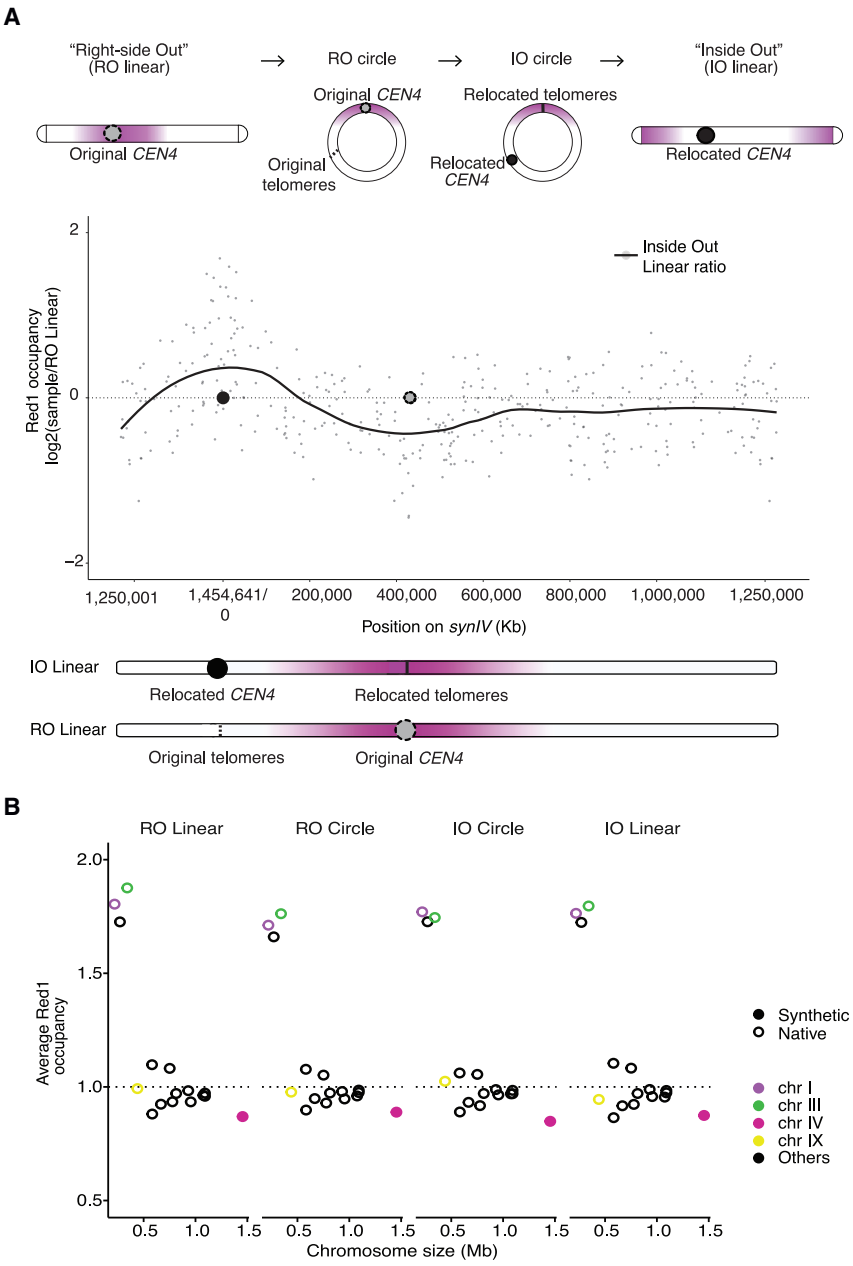

Figure 7. Meiotic axis protein Red1 occupancy changes upon centromere relocation

(A) Mean signal of Red1 peaks along engineered *synIV* chromosomes as $\log_2$-transformed ratio between inside-out linear and right-side-out linear. In the inside-out linear strains, *CEN4* was relocated to the original telomere positions, and the new telomeres are in the original centromere site. Points represent mean peak signal, and lines represent local regression (loess normalized). Note: chromosomal coordinates were shifted by approximately 200 kb for better visualization. The last 10 points from each end were appended to the other end to ensure that the local regression line is continuous across the ends.

(B) Red1 occupancy versus chromosome length in the S288c background of engineered *synIV* strains.

chromosome (*synIII-I*) have no growth defects or major transcriptomic changes, indicating that yeast tolerates both synthetic design changes and fusion chromosomes, as previous studies suggested.[1–7,9,18,23,30] Several other synthetic yeast chromosomes have also been successfully assembled and analyzed, marking a significant milestone for Sc2.0: the completion of assembly for all individual synthetic chromosomes.[31–38] The fusion strategy designed here can be easily adapted to building any synthetic fusion chromosomes in budding yeast.

As a consequence of building *synI* as part of Sc2.0, we have explored in detail a set of fusion chromosome strains. We attached wild-type *chrI* to three separate chromosomes with arms of different lengths, dramatically changing the neighbors that *chrI* interacted with most frequently in *trans*. In the extreme case, when attached to the long arm of *chrIV*, *chrI* interacted strongly with all long chromosome arms and much less with small arms. This is completely opposite of what is seen with native *chrI*. This finding provides direct evidence for a previous study related to DNA repair and genomic environment: the relocation of the same fragment to different-length chromosome arms changes the environment of the fragment, leading to differential efficiencies of homology searching and DNA repair.[39]

Despite significantly reorganized 3D structure, the synthetic fusion chromosome supported normal growth. These findings underscore the extreme tolerance of the yeast genome with respect to intranuclear 3D positioning. Previous work in which the rDNA cluster was relocated from *chrXII* to the much shorter *chrIII* supports this hypothesis.[7] The right arm of *chrIII* was split into two no-longer-interacting segments due to insertion of Mb-length rDNA array. No fitness defects were detected in that strain either, despite major rearrangement of multiple yeast chromosomes to accommodate ectopically located rDNA.[9] More recent studies also showed that yeast grow well even with dramatic rearrangements of yeast 3D genome structure by fusing 16 chromosomes into 1 or 2 giant chromosomes.[21,23] Together, these data reinforce the fact that the budding yeast genome is extremely plastic and tolerates surprisingly vast changes in 3D genome structure without obvious ill effects. Along the same lines, we showed here that "liberating" *synI* from the *synIII-synI* fusion chromosome context did not significantly affect fitness.

Hi-C analysis of the three fusion chromosome strains in mitotic cells revealed an unexpected loop formed between *HMR* and the

chrIR telomere of the *chrIII-I* fusion chromosome. This loop further constrains the *chrIX-III-I* fusion chromosome into a more twisted configuration. Specific long-range interactions between *HML* and *HMR* are known to depend on the SIR silencer protein complex.[40] A previous study revealed loss of specific long-range interactions between the silent mating type loci in *synIII* strains from which *HML* and *HMR* were removed by design.[9] Telomere silencing also requires binding of SIR proteins: confocal microscopic images show that in normal strains, telomeres are clustered into 6–8 foci at the nuclear periphery, sometimes overlapping with *HML* and/or *HMR*.[41] We hypothesize that the looped and twisted structures observed represent previously unknown *HML*, *HMR*, and telomere interactions held together or maintained at the nuclear periphery by silencing protein complexes. Consistent with this, when we deleted *SIR3* in the *chrIX-III-I* strain, the twisted structure disappeared.

In meiosis, chromosomes are packaged in a distinct manner to assure proper disjunction of homologs and the formation of double-strand breaks and, subsequently, chiasmata. Short chromosomes tend to have higher rates of meiotic recombination,[11] which may promote their faithful meiotic disjunction.[15] Multiple mechanisms cooperate to enrich recombination regulators on short chromosomes,[13–15,17] although the molecular mechanisms are poorly defined. Chromosome translocation experiments indicated that increased binding of double-strand break factors is partly encoded in *cis*.[15] Our analysis of fusion chromosomes indicates that *cis*-acting elements also promote relative enrichment of axial element components, as relative enrichment of Red1 on small chromosomes (*chrI*, *chrIII*) is retained when these sequences are placed into the context of much larger chromosomes.

Modeling of enrichment patterns has pointed to possible roles for telomeres and centromeres as mediating enrichment of recombination factors on small chromosomes.[15,17,42] Our analyses now show that deletion or inactivation of centromeres on small chromosomes leads to a profound reduction in Red1 binding on fusion chromosomes. Decreased Red1 binding extended approximately 100 kb to either side of inactivated centromeres. Although all tested centromeres show this effect, the long-range nature of the Red1 binding disproportionately affects small chromosomes. This provides an interesting paradigm for how a genetic element present on all chromosomes can nevertheless have a much more pronounced effect on small chromosomes and mirrors similar long-range effects observed near chromosome ends at late stages of meiotic recombination.[15,17,42]

Paradoxically, Red1 enrichment within 100 kb of centromeres is not elevated above the genome average on wild-type chromosomes[13] and drops substantially below genome average upon centromere inactivation. We speculate that this dependency reflects a need for equalizing Red1 binding along chromosomes. Centromeres are the first chromosomal regions to accumulate recombination-promoting proteins,[15,17,43] suggesting that centromeres may inherently promote meiotic recombination. However, excessive recombination near centromeres is deleterious,[44] which may favor local changes in genome sequence that reduce Red1 recruitment to balance Red1 levels along chromosomes (Figure S8). In support of this model, we show that locating a centromere into a region that has not yet gone through years of adaptation caused strong regional increase of Red1 signals in the new pericentromeric regions. Thus, our engineered strains suggest that Red1 enrichment around centromeres is shaped by opposing evolutionary pressures that prevent Red1 over-enrichment in the pericentromeric regions while still promoting the recombination factor enrichment on small chromosomes.

Here, we engineered a series of synthetic yeast fusion chromosomes with the smallest yeast chromosome, *chrI*. Through investigating these synthetic yeast fusion chromosomes, we uncovered previously unappreciated but strong interactions between *HML*, *HMR*, and telomeres in yeast genome architecture regulated by silencing protein Sir3. In addition, we elucidate the mechanism of how *chrI* and other small chromosomes specifically enhance meiotic recombination. Given the important role of centromeres in recruiting axial elements and forming meiotic crossovers especially for small chromosomes, mutations that weaken this centromere-mediated recruitment are expected to preferentially cause mis-segregation of short chromosomes and contribute to chromosomal birth defects, such as Down syndrome, typically caused by meiotic non-disjunction of chromosome 21, one of the smallest human chromosomes.[45] These experiments reveal the power of synthetic biology to uncover new biology and unravel complex biological systems.

Limitations of the study

We generated both "liberated" *synI* and fusion chromosome *synIII-I* strains, but we only examined growth of the former on rich media. To check for potential subtle growth defects, competition assays should be carried out for "liberated" *synI* and *chrI* strains that went through the same procedures. In addition, mitotic stability of "liberated" *synI* has not yet been measured.

Since Hi-C data represent an aggregate bulk result of numerous nuclei with potentially varying 3D structures, contact maps and 3D representations represent population averages. Thus, individual nuclei likely exhibit dynamic and diverse genome architecture. However, the 3D representation is a standard method to help general readers visualize structural feature differences.

CONSORTIA

This work is part of the international Synthetic Yeast Genome (Sc2.0) consortium. The chromosome design and building consortium includes research groups worldwide: Boeke Lab at Johns Hopkins University and New York University (led chromosomes I, III, IV, VI, VIII, and IX); Chandrasegaran lab at Johns Hopkins (led chromosomes III and IX); Cai Lab at University of Edinburgh and University of Manchester (led chromosomes II and VII and tRNA neochromosome); Yue Shen's team at BGI-Research SHENZHEN (led chromosomes II, VII, and XIII); Y.J. Yuan's team at Tianjin University (led chromosomes V and X); Dai Lab at Tsinghua University and Shenzhen Institute of Advanced Technology, CAS (led chromosome XII); Ellis Lab at Imperial College London (led chromosome XI); Sakkie Pretorius's team at Macquarie University (led chromosomes XIV and XVI); Matthew Wook Chang's team at National University of Singapore (led chromosome XV); Bader and Boeke Labs at

Johns Hopkins University (led design and workflow); and Build-A-Genome undergraduate teams at Johns Hopkins University and Loyola University Maryland (contributed to chromosomes I, III, IV, VIII, and IX). The Sc2.0 consortium includes numerous other participants who are acknowledged on the project website, www.syntheticyeast.org.

STAR★METHODS

Detailed methods are provided in the online version of this paper and include the following:

- KEY RESOURCES TABLE
- RESOURCE AVAILABILITY
  - Lead contact
  - Materials availability
  - Data and code availability
- EXPERIMENTAL MODEL AND STUDY PARTICIPANT DETAILS
  - Strains
- METHOD DETAILS
  - CRISPR-Cas9 method to fuse chromosomes
  - Telomerase mediated Precision Splitting
  - Whole genome sequencing and RNA seq
  - Hi-C libraries
  - Generation and normalization of contact maps
  - 3D representation inferred from contact maps
  - Synchronous meiosis and chromatin immunoprecipitation (ChIP)
  - Read alignment and peak calling
  - Recombination analysis

SUPPLEMENTAL INFORMATION

Supplemental information can be found online at https://doi.org/10.1016/j.xgen.2023.100439.

ACKNOWLEDGMENTS

We thank Beverley Wendland and Eliot McVeigh for their support of the Build-A-Genome course at Johns Hopkins University over many years. We thank the NYU Langone Health Genome Technology Center, especially A. Heguy, G. Westby, and P. Zappile, for deep-sequencing libraries, and Z. Kuang for advice on bioinformatic analyses. This work was supported by NSF grants MCB-1026068, MCB-1443299, MCB-1616111, and MCB-1921641 to J.D.B., NSF grant MCB-1445545 to J.S.B., the European Research Council (ERC) grant agreement 260822 to R.K., and funding from the National Institutes of Health (R35GM148223) and the March of Dimes Foundation (6-FY6-208) to A.H.

AUTHOR CONTRIBUTIONS

J.L. and J.D.B. conceived the project. L.A.M., J.D.B., and J.S.B. designed *synI*. J.L., R.K., A.H., and J.D.B. designed and analyzed the experiments. J.L.; G.M. and A.T. (in the lab of R.K.); L.A.V.-S., A.R.R., and J.H. (in the lab of A.H.); W.Z., N.A., Y.Z., C.C., L.H.M., S.L., and BAG students performed the experiments. G.S., J.C., and K.Y. (in the lab of J.S.B.) performed chromosome segmentation, carried out computational analyses, and uploaded final sequences to NCBI. X.S. (in the lab of J.D.B.); L.A.V.-S., A.R.R., and J.H. (in the lab of A.H.); G.M. (in the lab of R.K.); and J.M. performed computational analyses. J.L., A.H., and J.D.B. wrote the manuscript, and all authors contributed to its editing.

DECLARATION OF INTERESTS

J.D.B, L.A.M., and J.S.B. are founders of Neochromosome, Inc. J.D.B. is also a consultant of Neochromosome; a Founder and Director of CDI Labs, Inc,; a Founder of, Scientific Advisory Board member of, and consultant to ReOpen Diagnostics, LLC; and serves or served on the Scientific Advisory Board of the following: Logomix, Inc.; Sangamo, Inc.; Modern Meadow, Inc.; Rome Therapeutics, Inc.; Sample6, Inc.; Tessera Therapeutics, Inc.; and the Wyss Institute. N.A. is a synthetic biology specialist at Alagene.

Received: October 24, 2022
Revised: August 23, 2023
Accepted: October 13, 2023
Published: November 8, 2023

REFERENCES

1. Dymond, J.S., Richardson, S.M., Coombes, C.E., Babatz, T., Muller, H., Annaluru, N., Blake, W.J., Schwerzmann, J.W., Dai, J., Lindstrom, D.L., et al. (2011). Synthetic chromosome arms function in yeast and generate phenotypic diversity by design. Nature *477*, 471–476. https://doi.org/10.1038/nature10403.
2. Annaluru, N., Muller, H., Mitchell, L.A., Ramalingam, S., Stracquadanio, G., Richardson, S.M., Dymond, J.S., Kuang, Z., Scheifele, L.Z., Cooper, E.M., et al. (2014). Total synthesis of a functional designer eukaryotic chromosome. Science *344*, 55–58. https://doi.org/10.1126/science.1249252.
3. Mitchell, L.A., Wang, A., Stracquadanio, G., Kuang, Z., Wang, X., Yang, K., Richardson, S., Martin, J.A., Zhao, Y., Walker, R., et al. (2017). Synthesis, debugging, and effects of synthetic chromosome consolidation: synVI and beyond. Science *355*, eaaf4831. https://doi.org/10.1126/science.aaf4831.
4. Shen, Y., Wang, Y., Chen, T., Gao, F., Gong, J., Abramczyk, D., Walker, R., Zhao, H., Chen, S., Liu, W., et al. (2017). Deep functional analysis of synII, a 770-kilobase synthetic yeast chromosome. Science *355*, eaaf4791. https://doi.org/10.1126/science.aaf4791.
5. Wu, Y., Li, B.Z., Zhao, M., Mitchell, L.A., Xie, Z.X., Lin, Q.H., Wang, X., Xiao, W.H., Wang, Y., Zhou, X., et al. (2017). Bug mapping and fitness testing of chemically synthesized chromosome X. Science *355*, eaaf4706. https://doi.org/10.1126/science.aaf4706.
6. Xie, Z.X., Li, B.Z., Mitchell, L.A., Wu, Y., Qi, X., Jin, Z., Jia, B., Wang, X., Zeng, B.X., Liu, H.M., et al. (2017). Perfect" designer chromosome V and behavior of a ring derivative. Science *355*, eaaf4704. https://doi.org/10.1126/science.aaf4704.
7. Zhang, W., Zhao, G., Luo, Z., Lin, Y., Wang, L., Guo, Y., Wang, A., Jiang, S., Jiang, Q., Gong, J., et al. (2017). Engineering the ribosomal DNA in a megabase synthetic chromosome. Science *355*, eaaf3981. https://doi.org/10.1126/science.aaf3981.
8. Zhang, W., Lazar-Stefanita, L., Yamashita, H., Shen, M.J., Mitchell, L.A., Kurasawa, H., Lobzaev, E., Fanfani, V., Haase, M.A.B., Sun, X., et al. (2023). Manipulating the 3D organization of the largest synthetic yeast chromosome. Mol. Cell *83*. https://doi.org/10.1016/j.molcel.2023.10.015.
9. Mercy, G., Mozziconacci, J., Scolari, V.F., Yang, K., Zhao, G., Thierry, A., Luo, Y., Mitchell, L.A., Shen, M., Shen, Y., et al. (2017). 3D organization of synthetic and scrambled chromosomes. Science *355*, eaaf4597. https://doi.org/10.1126/science.aaf4597.
10. Belton, J.M., Lajoie, B.R., Audibert, S., Cantaloube, S., Lassadi, I., Goiffon, I., Baù, D., Marti-Renom, M.A., Bystricky, K., and Dekker, J. (2015). The Conformation of Yeast Chromosome III Is Mating Type Dependent and Controlled by the Recombination Enhancer. Cell Rep. *13*, 1855–1867. https://doi.org/10.1016/j.celrep.2015.10.063.
11. Kaback, D.B., Guacci, V., Barber, D., and Mahon, J.W. (1992). Chromosome size-dependent control of meiotic recombination. Science *256*, 228–232.

12. Kaback, D.B. (1996). Chromosome-size dependent control of meiotic recombination in humans. Nat. Genet. *13*, 20–21. https://doi.org/10.1038/ng0596-20.

13. Sun, X., Huang, L., Markowitz, T.E., Blitzblau, H.G., Chen, D., Klein, F., and Hochwagen, A. (2015). Transcription dynamically patterns the meiotic chromosome-axis interface. Elife *4*, e07424. https://doi.org/10.7554/eLife.07424.

14. Panizza, S., Mendoza, M.A., Berlinger, M., Huang, L., Nicolas, A., Shirahige, K., and Klein, F. (2011). Spo11-accessory proteins link double-strand break sites to the chromosome axis in early meiotic recombination. Cell *146*, 372–383. https://doi.org/10.1016/j.cell.2011.07.003.

15. Murakami, H., Lam, I., Huang, P.C., Song, J., van Overbeek, M., and Keeney, S. (2020). Multilayered mechanisms ensure that short chromosomes recombine in meiosis. Nature *582*, 124–128. https://doi.org/10.1038/s41586-020-2248-2.

16. Thacker, D., Mohibullah, N., Zhu, X., and Keeney, S. (2014). Homologue engagement controls meiotic DNA break number and distribution. Nature *510*, 241–246. https://doi.org/10.1038/nature13120.

17. Subramanian, V.V., Zhu, X., Markowitz, T.E., Vale-Silva, L.A., San-Segundo, P.A., Hollingsworth, N.M., Keeney, S., and Hochwagen, A. (2019). Persistent DNA-break potential near telomeres increases initiation of meiotic recombination on short chromosomes. Nat. Commun. *10*, 970. https://doi.org/10.1038/s41467-019-08875-x.

18. Richardson, S.M., Mitchell, L.A., Stracquadanio, G., Yang, K., Dymond, J.S., DiCarlo, J.E., Lee, D., Huang, C.L.V., Chandrasegaran, S., Cai, Y., et al. (2017). Design of a synthetic yeast genome. Science *355*, 1040–1044. https://doi.org/10.1126/science.aaf4557.

19. Bussey, H., Kaback, D.B., Zhong, W., Vo, D.T., Clark, M.W., Fortin, N., Hall, J., Ouellette, B.F., Keng, T., Barton, A.B., et al. (1995). The nucleotide sequence of chromosome I from Saccharomyces cerevisiae. Proc. Natl. Acad. Sci. USA *92*, 3809–3813.

20. Murray, A.W., Schultes, N.P., and Szostak, J.W. (1986). Chromosome length controls mitotic chromosome segregation in yeast. Cell *45*, 529–536.

21. Luo, J., Sun, X., Cormack, B.P., and Boeke, J.D. (2018). Karyotype engineering by chromosome fusion leads to reproductive isolation in yeast. Nature *560*, 392–396. https://doi.org/10.1038/s41586-018-0374-x.

22. Verstrepen, K.J., Jansen, A., Lewitter, F., and Fink, G.R. (2005). Intragenic tandem repeats generate functional variability. Nat. Genet. *37*, 986–990. https://doi.org/10.1038/ng1618.

23. Shao, Y., Lu, N., Wu, Z., Cai, C., Wang, S., Zhang, L.L., Zhou, F., Xiao, S., Liu, L., Zeng, X., et al. (2018). Creating a functional single chromosome yeast. Nature *560*, 331–335. https://doi.org/10.1038/s41586-018-0382-x.

24. van Berkum, N.L., Lieberman-Aiden, E., Williams, L., Imakaev, M., Gnirke, A., Mirny, L.A., Dekker, J., and Lander, E.S. (2010). Hi-C: a method to study the three-dimensional architecture of genomes. J. Vis. Exp. https://doi.org/10.3791/1869.

25. Duan, Z., Andronescu, M., Schutz, K., McIlwain, S., Kim, Y.J., Lee, C., Shendure, J., Fields, S., Blau, C.A., and Noble, W.S. (2010). A three-dimensional model of the yeast genome. Nature *465*, 363–367. https://doi.org/10.1038/nature08973.

26. Therizols, P., Duong, T., Dujon, B., Zimmer, C., and Fabre, E. (2010). Chromosome arm length and nuclear constraints determine the dynamic relationship of yeast subtelomeres. Proc. Natl. Acad. Sci. USA *107*, 2025–2030. https://doi.org/10.1073/pnas.0914187107.

27. Lesne, A., Riposo, J., Roger, P., Cournac, A., and Mozziconacci, J. (2014). 3D genome reconstruction from chromosomal contacts. Nat. Methods *11*, 1141–1143. https://doi.org/10.1038/nmeth.3104.

28. Rusche, L.N., Kirchmaier, A.L., and Rine, J. (2003). The establishment, inheritance, and function of silenced chromatin in Saccharomyces cerevisiae. Annu. Rev. Biochem. *72*, 481–516. https://doi.org/10.1146/annurev.biochem.72.121801.161547.

29. Deutschbauer, A.M., and Davis, R.W. (2005). Quantitative trait loci mapped to single-nucleotide resolution in yeast. Nat. Genet. *37*, 1333–1340. https://doi.org/10.1038/ng1674.

30. Luo, J., Sun, X., Cormack, B.P., and Boeke, J.D. (2018). Karyotype engineering by chromosome fusion leads to reproductive isolation in yeast. Nature *560*, 392–396. https://doi.org/10.1038/s41586-018-0374-x.

31. Zhao, Y., Coelho, C., Hughes, A.L., Lazar-Stefanita, L., Yang, S., Brooks, A.N., Walker, R.S.K., Zhang, W., Lauer, S., Hernandez, C., Cai, J., et al. (2023). Debugging and consolidating multiple synthetic chromosomes reveals combinatorial genetic interactions. Cell *186*, 13108. https://doi.org/10.1016/j.cell.2023.09.025.

32. Lauer, S., Luo, J., Lazar-Stefanita, L., Zhang, W., McCulloch, L.H., Fanfani, V., Lobzaev, E., Haase, M.A.B., Easo, N., Zhao, Y., et al. (2023). Context-dependent neocentromere activity in synthetic yeast chromosome *VIII*. Cell Genom. *3*, 100437. https://doi.org/10.1016/j.xgen.2023.100437.

33. McCulloch, L.H., Sambasivam, V., Hughes, A.L., Annaluru, N., Ramalingam, S., Fanfani, V., Lobzaev, E., Mitchell, L.A., Cai, J., et al.; The Build-A-Genome Class (2023). Consequences of a telomerase-related fitness defect and chromosome substitution technology in yeast *synIX* strains. Cell Genom. *3*, 100419. https://doi.org/10.1016/j.xgen.2023.100419.

34. Shen, Y., Gao, F., Wang, Y., Wang, Y., Zheng, J., Gong, J., Zhang, J., Luo, Z., Schindler, D., Deng, Y., et al. (2023). Dissecting aneuploidy phenotypes by constructing Sc2.0 chromosome VII and SCRaMbLEing synthetic disomic yeast. Cell Genom. *3*, 100364. https://doi.org/10.1016/j.xgen.2023.100364.

35. Blount, B.A., Lu, X., Driessen, M.R.M., Jovicevic, D., Sanchez, M.I., Ciurkot, K., Zhao, Y., Lauer, S., McKiernan, R.M., Gowers, G.-O.F., et al. (2023). Synthetic yeast chromosome XI design provides a testbed for the study of extrachromosomal circular DNA dynamics. Cell Genom. *3*, 100418. https://doi.org/10.1016/j.xgen.2023.100418.

36. Schindler, D., Walker, R.S.K., Jiang, S., Brooks, A.N., Wang, Y., Müller, C.A., Cockram, C., Luo, Y., García, A., Schraivogel, D., et al. (2023). Design, Construction, and Functional Characterization of a tRNA Neochromosome in Yeast. Cell *186*, 13126. https://doi.org/10.1016/j.cell.2023.10.015.

37. Williams, T.C., Kroukamp, H., Xu, X., Wightman, E.L.I., Llorente, B., Borneman, A.R., Carpenter, A.C., Van Wyk, N., Meier, F., Collier, T.R.V., et al. (2023). Parallel laboratory evolution and rational debugging reveal genomic plasticity to *S. cerevisiae* synthetic chromosome XIV defects. Cell Genom. *3*, 100379. https://doi.org/10.1016/j.xgen.2023.100379.

38. Foo, J.L., Kitano, S., Susanto, A.V., Jin, Z., Lin, Y., Luo, Z., Huang, L., Liang, Z., Mitchell, L.A., Yang, K., et al. (2023). Establishing chromosomal design-build-test-learn through a synthetic chromosome and its combinatorial reconfiguration. Cell Genom. *3*, 100435. https://doi.org/10.1016/j.xgen.2023.100435.

39. Agmon, N., Liefshitz, B., Zimmer, C., Fabre, E., and Kupiec, M. (2013). Effect of nuclear architecture on the efficiency of double-strand break repair. Nat. Cell Biol. *15*, 694–699. https://doi.org/10.1038/ncb2745.

40. Miele, A., Bystricky, K., and Dekker, J. (2009). Yeast silent mating type loci form heterochromatic clusters through silencer protein-dependent long-range interactions. PLoS Genet. *5*, e1000478. https://doi.org/10.1371/journal.pgen.1000478.

41. Taddei, A., and Gasser, S.M. (2012). Structure and function in the budding yeast nucleus. Genetics *192*, 107–129. https://doi.org/10.1534/genetics.112.140608.

42. Blitzblau, H.G., Bell, G.W., Rodriguez, J., Bell, S.P., and Hochwagen, A. (2007). Mapping of meiotic single-stranded DNA reveals double-stranded-break hotspots near centromeres and telomeres. Curr. Biol. *17*, 2003–2012. https://doi.org/10.1016/j.cub.2007.10.066.

43. Kugou, K., Fukuda, T., Yamada, S., Ito, M., Sasanuma, H., Mori, S., Katou, Y., Itoh, T., Matsumoto, K., Shibata, T., et al. (2009). Rec8 guides canonical Spo11 distribution along yeast meiotic chromosomes. Mol. Biol. Cell *20*, 3064–3076. https://doi.org/10.1091/mbc.E08-12-1223.

44. Vincenten, N., Kuhl, L.M., Lam, I., Oke, A., Kerr, A.R., Hochwagen, A., Fung, J., Keeney, S., Vader, G., and Marston, A.L. (2015). The kinetochore prevents centromere-proximal crossover recombination during meiosis. Elife *4*, e10850. https://doi.org/10.7554/eLife.10850.

45. Chen, Q., Tan, B., He, J.L., Liu, X.Q., Chen, X.M., Gao, R.F., Zhu, J., Wang, Y.X., and Qi, H.B. (2017). Mutational spectrum of CENP-B box and alpha-satellite DNA on chromosome 21 in Down syndrome children. Mol. Med. Rep. *15*, 2313–2317. https://doi.org/10.3892/mmr.2017.6247.

46. Robinson, J.T., Thorvaldsdóttir, H., Winckler, W., Guttman, M., Lander, E.S., Getz, G., and Mesirov, J.P. (2011). Integrative genomics viewer. Nat. Biotechnol. *29*, 24–26. https://doi.org/10.1038/nbt.1754.

47. Bolger, A.M., Lohse, M., and Usadel, B. (2014). Trimmomatic: a flexible trimmer for Illumina sequence data. Bioinformatics *30*, 2114–2120. https://doi.org/10.1093/bioinformatics/btu170.

48. Langmead, B., and Salzberg, S.L. (2012). Fast gapped-read alignment with Bowtie 2. Nat. Methods *9*, 357–359. https://doi.org/10.1038/nmeth.1923.

49. Zhang, Y., Liu, T., Meyer, C.A., Eeckhoute, J., Johnson, D.S., Bernstein, B.E., Nusbaum, C., Myers, R.M., Brown, M., Li, W., and Liu, X.S. (2008). Model-based analysis of ChIP-Seq (MACS). Genome Biol. *9*, R137. https://doi.org/10.1186/gb-2008-9-9-r137.

50. Mitchell, L.A., and Boeke, J.D. (2014). Circular permutation of a synthetic eukaryotic chromosome with the telomerator. Proc. Natl. Acad. Sci. USA *111*, 17003–17010. https://doi.org/10.1073/pnas.1414399111.

51. Lazar-Stefanita, L., Scolari, V.F., Mercy, G., Muller, H., Guérin, T.M., Thierry, A., Mozziconacci, J., and Koszul, R. (2017). Cohesins and condensins orchestrate the 4D dynamics of yeast chromosomes during the cell cycle. EMBO J. *36*, 2684–2697. https://doi.org/10.15252/embj.201797342.

52. Imakaev, M., Fudenberg, G., McCord, R.P., Naumova, N., Goloborodko, A., Lajoie, B.R., Dekker, J., and Mirny, L.A. (2012). Iterative correction of Hi-C data reveals hallmarks of chromosome organization. Nat. Methods *9*, 999–1003. https://doi.org/10.1038/nmeth.2148.

53. Cournac, A., Marbouty, M., Mozziconacci, J., and Koszul, R. (2016). Generation and Analysis of Chromosomal Contact Maps of Yeast Species. Methods Mol. Biol. *1361*, 227–245. https://doi.org/10.1007/978-1-4939-3079-1_13.

54. Cournac, A., Marie-Nelly, H., Marbouty, M., Koszul, R., and Mozziconacci, J. (2012). Normalization of a chromosomal contact map. BMC Genom. *13*, 436. https://doi.org/10.1186/1471-2164-13-436.

55. Morlot, J.B., Mozziconacci, J., and Lesne, A. (2016). Network concepts for analyzing 3D genome structure from chromosomal contact maps. Epj Nonlinear Biomed *4*, 2, UNSP 2. https://doi.org/10.1140/epjnbp/s40366-016-0029-5.

56. Humphrey, W., Dalke, A., and Schulten, K. (1996). VMD: visual molecular dynamics. J. Mol. Graph. *14*, 33–38, 27-28. https://doi.org/10.1016/0263-7855(96)00018-5.

57. Blitzblau, H.G., and Hochwagen, A. (2013). ATR/Mec1 prevents lethal meiotic recombination initiation on partially replicated chromosomes in budding yeast. Elife *2*, e00844. https://doi.org/10.7554/eLife.00844.

58. Yue, J.X., Li, J., Aigrain, L., Hallin, J., Persson, K., Oliver, K., Bergström, A., Coupland, P., Warringer, J., Lagomarsino, M.C., et al. (2017). Contrasting evolutionary genome dynamics between domesticated and wild yeasts. Nat. Genet. *49*, 913–924. https://doi.org/10.1038/ng.3847.

59. Langmead, B., Trapnell, C., Pop, M., and Salzberg, S.L. (2009). Ultrafast and memory-efficient alignment of short DNA sequences to the human genome. Genome Biol. *10*, R25. https://doi.org/10.1186/gb-2009-10-3-r25.

STAR★METHODS

KEY RESOURCES TABLE

REAGENT or RESOURCE	SOURCE	IDENTIFIER
Bacterial and viral strains		
TOP10 *E. coli* strain	Boeke lab collection	
Chemicals, peptides, and recombinant proteins		
Zymolyase 100T	US Biological	Z1004
Lithium acetate dihydrate	Sigma-Aldrich	L6883
Polyethylene glycol	Sigma-Aldrich	81188
Herring sperm DNA	Promega	D1816
Potassium acetate	Fisher	BP364
Zinc acetate dihydrate	Sigma-Aldrich	Z0625
(S)-(+)-Camptothecin	Sigma-Aldrich	C9911
D-Sorbitol	Sigma-Aldrich	S1876
6-Azauracil	Sigma-Aldrich	A1757
Hydroxyurea	Sigma-Aldrich	H8627
Methyl methanesulfonate	Sigma-Aldrich	129925
Methyl 1-(butylcarbamoyl)-2-benzimidazolecarbamate (Benomyl)	Sigma-Aldrich	381586
Cycloheximide	Sigma-Aldrich	01810
Hydrogen peroxide	Millipore	88597
GoTaq Green Master Mix	Promega	M7123
Phusion Hot Start Flex 2X Master Mix	Thermo Fisher Scientific	M0536
RNase A	Thermo Fisher Scientific	EN0531
Formaldehyde solution	Sigma-Aldrich	F8775
Biotin-14-dCTP	Invitrogen	19518018
Klenow enzyme	NEB	M0210L
T4 DNA ligase	Thermo Scientific	EL0014
Proteinase K	Thermo Scientific	EO0491
Invitrogen™ Dynabeads™ MyOne™ Streptavidin C1	Invitrogen	65001
KAPA-HiFi	Kapa Biosystems	KK2602
Formaldehyde solution	Sigma-Aldrich	F1635
Glycine	Sigma-Aldrich	G7126
Glass beads, acid washed	Sigma-Aldrich	G8772
Trizma base	Sigma-Aldrich	T4661
Ethylenediaminetetraacetic acid	Sigma-Aldrich	RDD017
Sodium Dodecyl Sulfate (SDS), Ultra Pure	American Bioanalytical	AB01920-01000
Phosphate-Buffered Saline	Corning	21-040-CV
GammaBind G Sepharose	GE Healthcare Bio	17-0885-01
Glycogen (5 mg/mL)	Ambion	AM9510
Proteinase K, 20 mg/ml solution	Amresco Inc.	E195
Lithium chloride	Sigma-Aldrich	L9650
RNase A (Ribonuclease A) in buffered glcerol solution	Sigma-Aldrich	R4642
dNTP Mixture (each 2.5 mM)	Takara	4030
T4 Polynucleotide Kinase (10,000 units/ml)	New England BioLabs	M0201S
Klenow Fragment	New England BioLabs	M0210S
T4 DNA Polymerase	New England BioLabs	M0203S

(*Continued on next page*)

Continued

REAGENT or RESOURCE	SOURCE	IDENTIFIER
dATP (100 mM)	ThermoFisher Scientific	10216018
Klenow Fragment exo-	New England BioLabs	M0212S
Agencourt AMPure XP	Beckman Coulter	A63880
Quick Ligase	New England BioLabs	M2200S
dNTP Mix (each 10 mM)	ThermoFisher Scientific	R0192
Phusion™ High-Fidelity DNA Polymerase (2 U/μL)	ThermoFisher Scientific	F-530XL
SeaKem LE Agarose	Lonza (via Fisher Scientific)	BMA50004
TrackIt 100bp DNA ladder	ThermoFisher Scientific	10488–058
Critical commercial assays		
Zyppy Plasmid Miniprep Kit	Zymo Research	D4037
Fungi/Yeast Genomic DNA Isolation Kit	Norgen	27300
NEBNext Ultra II FS DNA Library Kit	NEB	E7805
Zymoclean™ Large Fragment DNA Recovery	Zymo Research	D4046
RNeasy Mini Kit	QIAGEN	74106
NEBNext Ultra II RNA Library Prep Kit	NEB	E7770
Qubit RNA BR Assay Kit	Thermo Fisher Scientific	Q10210
NextSeq 500/550 High Output Kit v2.5 (75 Cycles)	Illumina	20024906
NextSeq 500/550 High Output Kit v2.5 (150 Cycles)	Illumina	20024907
TruSeq Nano DNA LT, Set A and B	Illumina, Inc.	FC-121-4001,FC-121-4002
Qubit dsDNA HS Assay Kit	Life Technologies (Invitrogen)	Q32851
MiniElute PCR Purification Kit	Qiagen	28004
Agilent TapeStation HS D1000 (DNA) Reagents	Agilent	5067–5585
Agilent TapeStation HS D1000 (DNA) Tape	Agilent	5067–5584
Qiaquick gel extraction kit (50 columns)	Qiagen	28704
KAPA Library Quantification Kit - Complete Kit (Universal)	Roche Applied Science	7960140001
Experimental models: Organisms/strains		
Saccharomyces cerevisiae: BY4741 and BY4742	Jef Boeke's laboratory	N/A
All other strains used in this study are listed in Table S3	N/A	N/A
Oligonucleotides		
Primers and gRNA sequences are listed in Table S5	N/A	N/A
Software and algorithms		
R	R Core Team	https://www.R-project.org/
Rstudio v1.3.1093	Rstudio	https://www.rstudio.com
Integrated Genomics Viewer (IGV) v2.7.2	Broad Institute	http://software.broadinstitute.org/software/igv/ [46]
Trimmomatic v0.39		http://www.usadellab.org/cms/index.php?page=trimmomatic [47]
Bowtie 2 v2.2.9		http://bowtie-bio.sourceforge.net/bowtie2/index.shtml [48]
ShRec3d		https://sites.google.com/site/julienmozziconacci/#TOC-Downloads.[27]
PyMol	Molecular Graphics System, Version 2.0 Schrodinger, LLC	
MACS v2.1.1		(https://github.com/taoliu/MACS/;[49]
Other		
Resource website for Sc2.0	N/A	https://syntheticyeast.github.io/
Data sources	N/A	GEO: BioProject PRJNA351844

RESOURCE AVAILABILITY

Lead contact

Further information should be directed to and will be fulfilled by the lead contact Jef D. Boeke (jef.boeke@nyulangone.org).

Materials availability

All unique/stable reagents generated in this study are available from the lead contact with a completed Materials Transfer Agreement.

Data and code availability

- Data reported in this paper have been deposited to the overarching Sc2.0 umbrella BioProject PRJNA351844. The data for *synI* are provided under Bioproject PRJNA899531. The specific data reported here for RNA-seq were deposited to Gene Expression Omnibus accession number GSE242509. The sequence of *synIII-I* is available at GenBank (CP111106). Raw sequencing data and fragment pileup files related to Chip-seq data are deposited at GEO (GSE114731).
- All code used to analyze the Chip-seq data is openly available online at https://github.com/hochwagenlab/Chr_fusion_hybrids.

EXPERIMENTAL MODEL AND STUDY PARTICIPANT DETAILS

Strains

All strains generated in this study are listed in Table S3 and different versions of synthetic chromosome 1 are listed in Table S6. For wild-type fusion chromosome strains, they are all derived from BY4741 (*MATa his3Δ0 leu2Δ0 met15Δ0 ura3Δ0)* by CRISPR-Cas9 editing. For *synI* strain construction, the starting strain is *synIII* (YLM422: *MATα his3Δ1 leu2Δ0 lys2Δ0 ura3Δ0 SYN3-272123bp HO::synSUP61*).[2] For Red1 ChIP-seq experiments, hybrid diploids were generated by mating fusion chromosome strains (*MATa*) to SK1 strain (*MATα ho::LYS2, lys2, ura3, leu2::hisG, his3::hisG, trp1::hisG*).

METHOD DETAILS

CRISPR-Cas9 method to fuse chromosomes

A KanMX cassette was first inserted into the subtelomere region of a chromosome arm to which *chrI* was to be fused. Then we used a previously developed CRISPR-Cas9[21] to generate cuts near the *chrIL* telomere, *CEN1* and inside the *KanMX* coding sequence, and provided two donors: one donor with ~400bp homology sequences to the *chrIL* subtelomere and the chromosome arm to be fused, and another donor carrying ~400bp homology sequences flanking *CEN1*. The primers that we used to amplify 400 bp homology sequences are provided in Table S5. The 20nt gRNA of KanMX is 5′-CTTCGTACGCTGCAGGTCGA-3′, and the 20nt gRNA of *CEN1* is 5′-AAGAAAGTTATATGTGTGAC-3'. *Chr1L*-gRNA sequence is 5′-CTCAATGTACGCGCCAGGCA-3'. Two telomeres and *CEN1* were deleted in each fusion experiment.[21] We first screened colonies for "winner" candidates by replica plating to YPD+G418 to select colonies sensitive to G418, followed by PCR verifications as previously described.[21] Note, for *chrIX-I* strain, it was generated by two steps yeast transformation rather than using CRISPR-Cas9. First step, we inserted a fragment carrying ~400bp homology sequence to left arm of chrI and a *URA3* selection marker into *chrIX* right arm near telomeres by homology recombination. Second step, we transformed cells with a fragment containing a *HIS3* marker flanking by ~400bp homology sequences around *CEN1*. Then we selected for cells that grow on SC–His plate and PCR verified the fusion of two chromosomes.

Telomerase mediated Precision Splitting

We inserted the telomerator into the boundary of synIII-I chromosome, as previously described,[50] except the final step. Rather than induced in liquid, we transformed a PCR purified wild-type CEN1 donor (Forward primer (5'->3′): CACTATTTGTACGA GTTCGTCAGG, Reverse primer (5'->3′): GGACTCACTCTGGCTGAATC) into the telomerator strain already carrying the pRS413-pGAL1-1-SceI plasmid, and selected on SC–His + Galactose plates. We verified the splitting of synIII and synI with PCR, nanopore sequencing, and pulse-field gel electrophoresis.

Whole genome sequencing and RNA seq

The libraries preparation of whole genome sequencing and RNA seq of the strain yJL632, as well as Data analysis was performed as previously described,[21] except that the libraries were sequenced as 150 bp single-end reads on an Illumina NextSeq 500. The thresholds we used for differentially expressed genes are p value $<10^{-3}$ and log 2|fold change| > 2.

Hi-C libraries

Hi-C libraries were generated using the *Dpn*II restriction enzyme and following the same protocol as the one described.[51] The resulting libraries were used as template and processed for 2x75 bp pair-end sequencing on an Illumina NextSeq500 according to manufacturer's instructions.

Generation and normalization of contact maps

Illumina sequencing data were processed as described.[51] First, PCR duplicates were removed. Second, each read of a pair was aligned independently with Bowtie 2.1.0 (mode: –very-sensitive –rdg 500,3 —rfg 500,3) and using an iterative procedure as described[52] against the genome of the corresponding fusion strain. Third, unwanted molecules (i.e., corresponding to loops, non-digested fragments, etc.; for details see[53,54]) were discarded. Finally, the remaining valid reads were binned into units of single restriction fragments, then successive fragments were assigned to fixed size bins of 5 kb. Contact maps were then normalized using the sequential component normalization procedure (SCN).[54] The contact ratios were computed between normalized maps binned at 50 kb.

3D representation inferred from contact maps

The 3D representations of the contact maps were generated using ShRec3D[27] on the normalized contact maps filtered for low signal bins. Each element of the normalized contact maps was inverted to compute sparse distance matrices. These matrices were then completed using the shortest path algorithm. 3D coordinates were then determined by multidimensional scaling using the Sammon mapping.[55] All 3D structures were rendered using VMD.[56]

Synchronous meiosis and chromatin immunoprecipitation (ChIP)

To induce synchronous meiosis, strains were pre-inoculated at OD_{600} = 0.3 in BYTA medium (1% yeast extract, 2% tryptone, 1% potassium acetate, 50 mM potassium phthalate) and grown for 16.5 h at 30°C. Cells were then washed twice with water, resuspended at OD_{600} = 2.0 in SPO medium (0.3% potassium acetate, pH 7.0) and incubated at 30°C. After 3 h incubation, 25-mL samples were harvested and fixed for 30 min in 1% formaldehyde. The formaldehyde was quenched with 125 mM glycine and samples were further processed as described previously.[57] One-tenth of the cell lysate was removed as an input sample and the remainder was immunoprecipitated for 16 h at 4°C with 2 μL of anti-Red1 serum (Lot#16440; kindly provided by N. Hollingsworth), followed by capture on GammaBind G Sepharose beads (GE Healthcare Bio).

Read alignment and peak calling

The hybrid genome was built by concatenating published assemblies of *S. cerevisiae* SK1 and S288c genomes.[58] For *synIV* strains, the hybrid genome was built by concatenating genome assemblies of SK1 and S288c with the syn4 chromosome. To make downstream visualization better, the fasta file of *synIV* was modified such that the last ~200 kb was shifted and attached to the start of the chromosome.

All sequencing reads were aligned to a concatenated hybrid genomes using Bowtie v1.2.0.[59] Only reads aligning perfectly (no mismatches, flag "-v 0") at a single position (flag "-m 1") were considered. Reads that do not overlap an SNP between SK1 and S288c will align to both genomes, becoming multimappers which were discarded. Regions with enriched Red1 protein signal (Red1 peaks) were identified using MACS v2.1.1[49] with command "macs2 callpeak". A "No shifting" model was built (flag "–nomodel") and reads were extended toward the 3′ direction to a fixed fragment length of 200 (flag "–extsize 200"). Flag "–SPMR" was set, in order to generate fragment pileups per million reads. The mappable genome size was set to 24 Mb (flag "–gsize 2.4e7") and default values were used for all other options. Input-corrected fragment pileups were generated with command "macs2 bdgcmp" and the fold enrichment method (flag "-m FE"). For Figure 6, Red1 occupancy is represented by the input and sequencing depth-normalized fragment pileup (fragment pileup per million reads), further normalized to mean Red1 occupancy on SK1 chromosomes. The smoothening used for Figures 7 and S5 was 0.5.

Recombination analysis

Heterozygous diploids were sporulated overnight in 2% potassium acetate solution at 25°C and then treated for 20 min at 37°C with zymolyase (USBiological, 1 mg/mL in 1M sorbitol), to digest the ascus walls. Tetrads were dissected on YPD plates by micromanipulation. Marker segregation of complete tetrads (all four spores viable) were determined by replica plating on selective media plates, following which the numbers of parental ditype (PD), non-parental ditype (NPD), tetratype (TT) were scored and used to calculate the recombination frequency.